Supplementary Information (SI) for Materials Horizons.
This journal is © The Royal Society of Chemistry 2024

Supplementary information for

Incarcerating Bismuth Nanoparticles into a Thiol-Laced Metal-Organic Framework for Electro and Photocatalysis

Parijat Borah *[a†], Natalie McLeod [a,b†], Nipun Kumar Gupta [a], Reuben J. Yeo [a], Tanmay Ghosh [a], Zainul Aabdin [a], Lidao Li [a], Prajna Bhatt [b], Yuhan Liu [b], Robert Palgrave [b], Yee-Fun Lim [c], Zhengtao Xu*[a] and Albertus Denny Handoko*[c]

[a] *Institute of Materials Research and Engineering (IMRE), Agency for Science, Technology and Research (A*STAR), Singapore 138634, Republic of Singapore. Email: Parijat_borah@imre.a-star.edu.sg, Zhengtao@imre.a-star.edu.sg*

[b] *Department of Chemistry, Christopher Ingold Building, 20 Gordon St., WC1H 0AJ, London, United Kingdom*

[c] *Institute of Sustainability for Chemicals, Energy and Environment (ISCE²), Agency for Science, Technology and Research (A*STAR), 1 Pesek Road, Jurong Island, Singapore 627833, Republic of Singapore, Email: Handoko_Albertus@isce2.a-star.edu.sg*

Table of content

Experimental section

Materials:

Starting materials, reagents, and solvents were purchased from commercial sources (Merk–Sigma Aldrich) unless otherwise specified and used without further purification. $ZrCl_4$ was purchased from Macklin, and 2,5-dimercapto-1,4-benzenedicarboxylic acid (H_2DMBD) was purchased from Henan Alfa Chemical Co. Ltd, China.

Characterization techniques:

Powder X-ray diffraction (PXRD) data was collected in the reflection mode at room temperature on a Bruker D8 Advance X-ray diffractometer with a Cu Kα radiation (λ = 1.5418 nm). A motorised divergence slit is programmed to achieve fixed sample X-ray illumination, therefore enhancing the signal intensities at higher 2θ range.

Quantitative refinements of PXRD data were done using DIFFRACplus TOPAS v4.2 (Bruker AXS GmbH), using crystallographic information file (CIF) of Zr-DMBD obtained from CCDC (deposition number 2091228). Only the lattice parameters, crystallite size, zero error, Zr atomic positions and the combined isotropic thermal parameters are allowed to relax to avoid significant change to the reference structure.

FT-IR spectra were recorded using a high resolution attenuated total reflectance (ATR)-IR Bruker Vertex 80v spectrophotometer in the range 400-4000 cm^{-1} with the sample powder.

BET surface areas were obtained using a Micromeritics ASAP 2020M automated high resolution micropore physisorption analyser.

To prepare the samples for TEM measurement, 2 µL sample solution was dropped on a standard carbon-coated Cu TEM grid. Samples were then naturally dried under ambient conditions before loading inside the TEM. A standard low-background double tilt holder (Thermo Fisher Scientific, Waltham, MA USA) is used to load the samples. The whole measurements were performed using Titan 80-300 keV and Tecnai G2 80-200 keV TEMs (Thermo Fisher Scientific, Waltham, MA USA). Titan with a 4096×4096 square pixels One View CMOS camera (Gatan, Inc., Pleasanton, CA, USA) is implemented for the imaging. The high-angle annular dark field images of Scanning transmission electron microscope (STEM) were acquired using Tecnai with an Annular Dark Field (ADF) detector (Fischione Instruments, Inc., PA USA).

X-ray photoelectron spectroscopy (XPS) was carried out on a Kratos Axis Supra+ system with monochromatic Al Kα radiation (hν = 1486.6 eV) used as the X-ray source. Photoelectrons were acquired from a region of 700 µm × 300 µm on the powder samples. The pass energy and step size used were 20 eV and 0.1 eV respectively for the high-resolution C 1s, O 1s, Bi 4f, and Zr 3d scans. During the measurements, an electron flood gun was used to neutralize any surface charges on the samples to prevent sample charging.

Thermo Gravimetric Analysis (TGA) was carried out on a TA Instrument TGA Q500 unit using a heating rate of 10 K/min under air flow of 60 ml/min. UV/vis spectra were obtained by using a Shimadzu UV-3600 UV–vis–NIR spectrometer.

UV-visible diffuse reflectance spectroscopy (DRS) was performed using integrating sphere attachment (Shimadzu MPC-3100).

Scanning Electron Microscopy (SEM) was carried out on a Hitachi SU8220 field emission scanning electron microscopy with an acceleration voltage of 5 kV under Secondary Electron (SE) mode.

Trace metal analyses were conducted by Inductively Coupled Plasma Mass Spectrometry (ICP-MS) using Agilent Technologies ICPMS 7700x machine. An Elemental Analyzer by Thermo Scientific Flash is used to measure elemental composition of C, H, N, S by combustion and separation of gases by column chromatography.

Electrochemical CO_2 reduction reaction (CO_2RR)

To prepare catalyst electrode, 5 mg of the Bi@Zr-DMBD-1 or BiNP@Zr-DMBD-2 powders were dissolved in 600 µL of DI water, 400 µL of ethanol, and 40 µL of Nafion™ ionomer. Subsequently, the suspension was ultrasonicated using pulse mode in an ice bath for 15 mins. Afterwards, the solution was mixed further using a vortex homogenizer (Ultra-Turrax), and 88 µL of this ink was then deposited onto 15 mm diameter glassy carbon disc and dried under an infrared lamp.

Static CO_2RR experiments were performed in a custom-made H-cell with 10 mL volume each in the anodic and cathodic compartment. A cationic exchange membrane (CMVN Selemion, AGC Engineering Co. Ltd.) was used as a barrier between the cathodic and anodic chambers in the H-Cell. 0.1 M $KHCO_3$ was used as electrolyte for CO_2RR. The electrolyte was subjected to pre-electrolysis cleaning treatment prior to use. 8 ml of the 0.1 M $KHCO_3$ electrolyte was injected into the anodic and cathodic chambers of the H-cell respectively and purged with ultrapure CO_2 at 20 sccm (Alicat MC-100 series).

Gaseous product quantification was performed using online Agilent 8980B GC equipped with programmable switch valves, packed mol sieve 5A and PLOT columns, methanizer, TCD, and FID detector. Online GC measurement began only after 10 minutes of CO_2 pre-saturation and 100 seconds of chronoamperometry current stabilization. Liquid product quantification was done using ^{1}H NMR (JEOL ECA II 500 MHz):

For the NMR sample preparation, 100uL of D_2O was added to 500uL of the combined electrolyte, along with 25uL of internal standard stock solution (5mM DMSO, 25mM phenol $_{(aq)}$), this mixture was then homogenized using the vortex homogenizer. DANTE pre-saturation water suppression was used during the data collection.

The glassy carbon disc coated with BiNP@Zr-DMBD acted as the working electrode (WE), with an Ag/AgCl leakless electrode (eDAQ) used as the reference (RE) and a pure graphite rod (Spec-Pure, Ted Pella) used as the counter electrode (CE). Voltage control was achieved using a Gamry 600+ potentiostat working in the chronoamperometry control. iR compensation was achieved using positive feedback (PF) correction mode at 85% of the pre-measured solution resistance (R_u). The R_u measurement was done using a single point impedance measurement at 100 kHz at -0.2 V DC voltage. The reference electrode was calibrated using hydrogen reference electrode (Hydroflex, Gaskatel GmbH) after considering the solution pH (6.81). Voltages in this work is expressed against reversible hydrogen electrode (RHE) unless specified.

3 compartment flow cell experimental procedure

Catalyst for the flow cell is prepared onto Sigracet 39-BB carbon paper substrate. Stock solution of catalyst ink is prepared using 24 mg of catalyst, 85 µL of 5% Nafion 117 solution (Sigma Aldrich) and 0.5 mL ethanol. The solution was mixed and sonicated for 20 mins in an ice bath, and then spray-coated onto the microporous layer of the carbon paper substrate, whilst ensuring not to saturate the substrate which would impair the gas diffusion layer. Achieving a catalyst loading of 0.5 mg cm^{-2}.

Flow CO_2RR was performed on a custom made 3-compartment flow cell. 25 mL solution of 1 M KOH was used as the anolyte and catholyte. The liquid flow rates for the anolyte and catholyte were approximately 30 mL/min (Kamoer Peristaltic Pump 550). The gas compartment CO_2 flow rate is set at 20 sccm. Fumasep FAA-3-PK-130 membrane was used for separating anode and cathode compartment. Experiments were run in chronopotentiometry mode at fixed current of 25 mA cm^{-2} using Autolab PGSTAT302N potentiostat.

Electrochemical analysis

Electrochemical surface area (ECSA) estimation was done by running variable scan rate cyclic voltammetry from 100 to 300 mV s^{-1} scan speed in 10 mV s^{-1} increment from 0.11 to 0.21 V voltage window was performed on BiNP@Zr-DMBD samples deposited on glassy carbon. CV scans were repeated three times, and the last scan was taken for calculation. The slope of current, taken at the end of CV scan with respect to scan speed is then taken as the estimate for double layer capacitance value representative of relative ECSA. More details can be seen in Supplementary Figure S13.

Variable DC bias electrochemical impedance spectroscopy (EIS) was performed with Gamry Reference 3000 on Bi@Zr-DMBD samples deposited on glassy carbon. DC bias was set at progressively from 0 V to -1.6 V with 0.05 V interval. AC signals with 10 mV magnitude was applied from 0.2 Hz to 100 kHz at 10 points per decade. A PTFE open cell filled with 1 M $KHCO_3$ saturated with CO_2 was used. CO_2 bubbling was stopped during EIS measurement to reduce noise. EIS fitting was done using Gamry Echem Analyst (version 7.10.1). Simplex optimization algorithm was used. Modified Anderson circuit equivalent with an additional parasitic R/C component was used as electrical equivalent model (see Supplementary Figure S14 for details).

Photocatalytic degradation of MB dye molecules

The photocatalytic activities of the prepared BiNP@Zr-DMBD-1 was for the degradation of methylene blue (MB) dye when exposed to visible light (specifically, blue light). In a typical experimental, 5 mg of BiNP@Zr-DMBD-1 was dispersed in a 10 ml aqueous solution containing 25 ppm of MB dye, and the mixture was continuously stirred while being subjected to blue LED light (PLS-LED 100C by PerfectLight) over a time interval. Subsequently, the photodegraded samples were centrifuged to separate the supernatant, and absorbance was recorded at λ_{max} = 661.0 nm using UV–vis spectrophotometer.

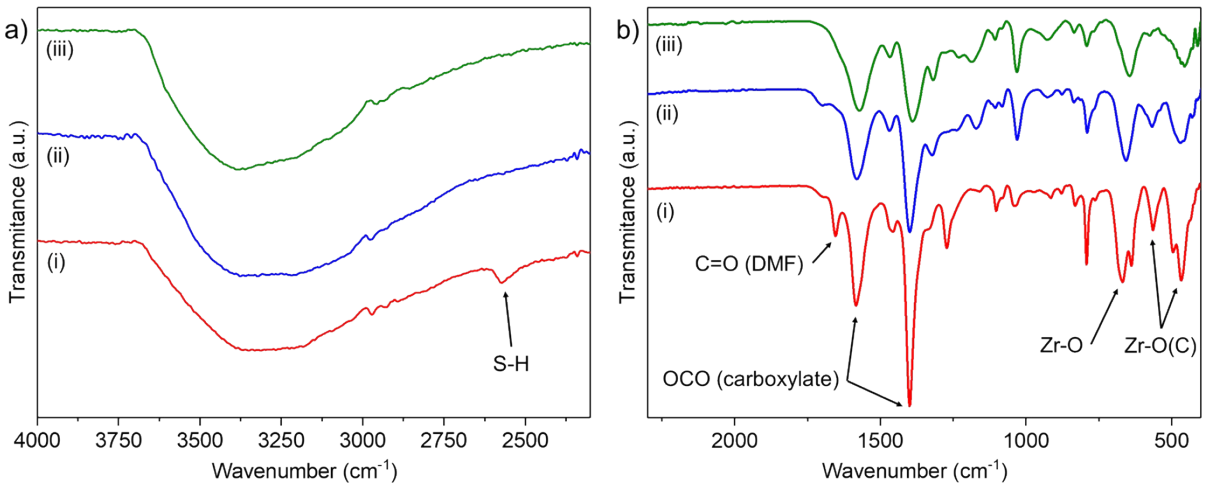

Figure S1. FT-IR spectra of (i) Zr-DMBD, (ii) Bi@Zr-DMBD, and (iii) BiNP@Zr-DMBD-1.

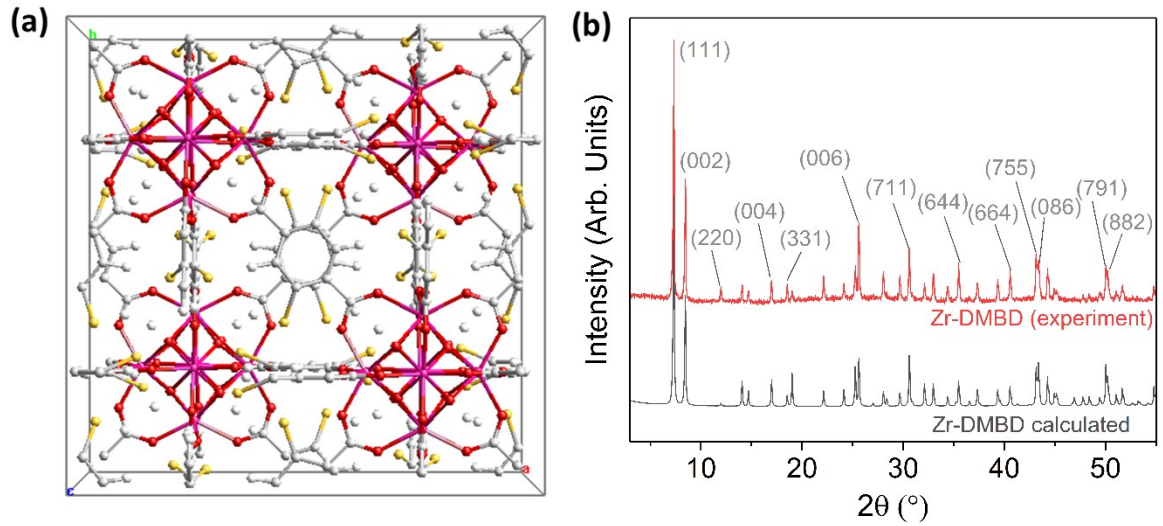

Figure S2. a) Simulated crystal structure of Zr-DMBD in ball-and-stick style generated using Topas, where balls in purple: zirconium; red: oxygen; yellow: sulfur; grey: carbon; white: hydrogen. b) XRD patterns of red line: experiment Zr-DMBD PXRD and grey line: quantitative refinement fitting using CIF obtained from CCDC (deposition number: 1405740). Ten highest intensity peaks were labelled.

Note: The CIF of Zr-DMBD is obtained from CCDC depository (2091228) deposited by B. Guo et al. [1] and used to perform quantitative analysis of the PXRD. Simple refinement, in fundamental parameter considering the obtained machine parameters using NIST SRM 640c was performed. Relaxed parameters include zero error, lattice parameters, crystallite size (Lorentzian), Zr "x" atom positions, and combined isotropic thermal parameters were performed. The refined cell parameters were 20.8458(±0.0009) Å.

B. Guo *et al.* reported a simulated structure for Zr-DMBD, identified through high-throughput screening of C_{24}^{12}= 2704156 candidate models based on UiO-66's structure. This model, with space group *F*23, was determined to be the most suitable structural representation of Zr-DMBD to date.

[1] B. Guo, X. Cheng, Y. Tang, W. Guo, S. Deng, L. Wu, X. Fu, Dehydrated UiO-66$(SH)_2$: The Zr–O Cluster and Its Photocatalytic Role Mimicking the Biological Nitrogen Fixation, *Angew. Chem. Int. Ed.* **2022**, *61, e202117244.*

Table S1: Data from the elemental compositions (C, H, N, S Elemental analysis and trace metal analyses by ICP-MS) of different MOF materials.

S No	Sample name	C,H,N,S Elemental analysis (wt%)				ICP-MS (wt%)		Zr/Bi
		Carbon	Nitrogen	Sulfur	Hydrogen	Zirconium	Bismuth	
1	Zr-DMBD	25.5	0.61	16.1	2.8	23.1	0	NA
2	Zr-DMBD ($NaBH_4$)[a]	22.1	0.32	14.6	3.4	21.8	0	NA
3	Bi@Zr-DMBD	17.0	0.05	11.3	1.6	16.0	25.1	6.0: 4.1
4	BiNP@Zr-DMBD-1	14.8	0.02	9.8	1.5	18.7	31.5	6.0: 4.4
5	BiNP@Zr-DMBD-1[b]	NA	NA	NA	NA	7.8	14.1	6.0: 4.7

[a] Zr-DMBD ($NaBH_4$): 60 mg of Zr-DMBD was dispersed in 10 ml of ice-cold DI water and the mixture was stirred in an ice bath for 30 min. To this, 2 mL of ice-cold aqueous $NaBH_4$ (1 M) was added dropwise and the reaction mixture was stirred at room temperature for 15 min. Afterward, the solid was isolated by centrifugation, washed with H_2O (10 mL, three times), and then with ethanol (10 mL, three times). The sample was immersed in acetone (replaced solvent three times in random intervals) for

one day for solvent exchange. Finally, the solids were dried under vacuum for 24 h at room temperature to obtain as-synthesized Zr-DMBD ($NaBH_4$).

[b] BiNP@Zr-DMBD-1: After electrochemical CO_2RR, BiNP@Zr-DMBD-1 was recovered from the electrode by sonication in ethanol, followed by centrifugation. It was then washed with ethanol and centrifuged again to remove as much Nafion as possible.

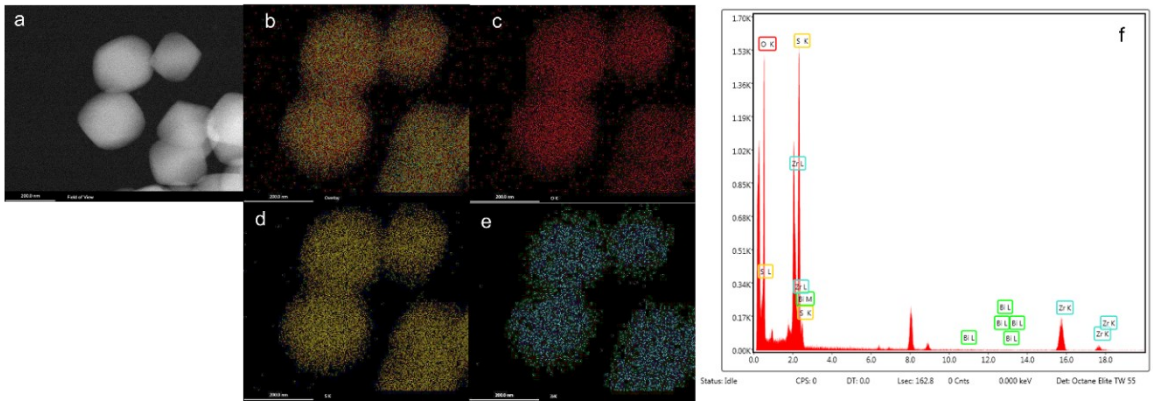

Figure S3: EDX mapping of Zr-DMBD: a) field of view, b) overlay, c) oxygen, d) sulfur, e) zirconium, and f) EDX signal spectrum.

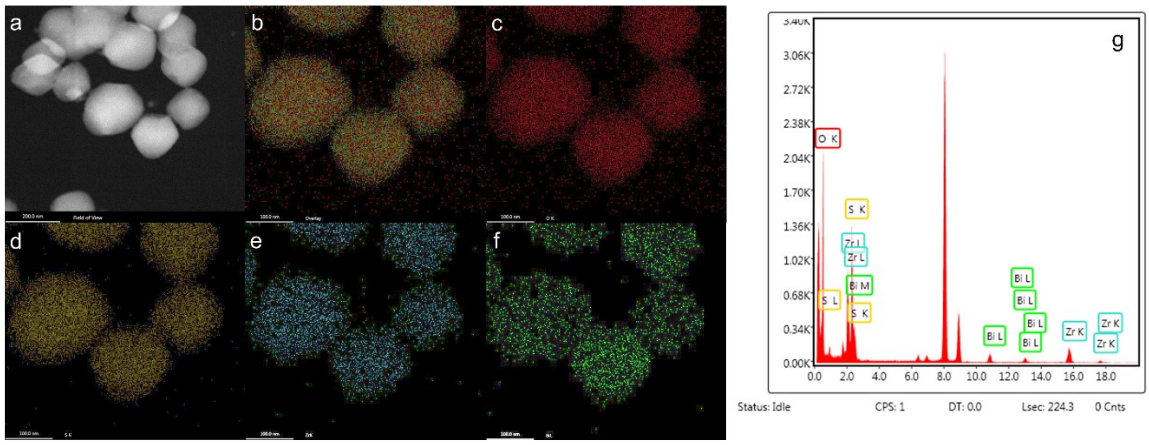

Figure S4. EDX mapping of Bi@Zr-DMBD: a) field of view, b) overlay, c) oxygen, d) sulfur, e) zirconium, f) bismuth, and g) EDX signal spectrum.

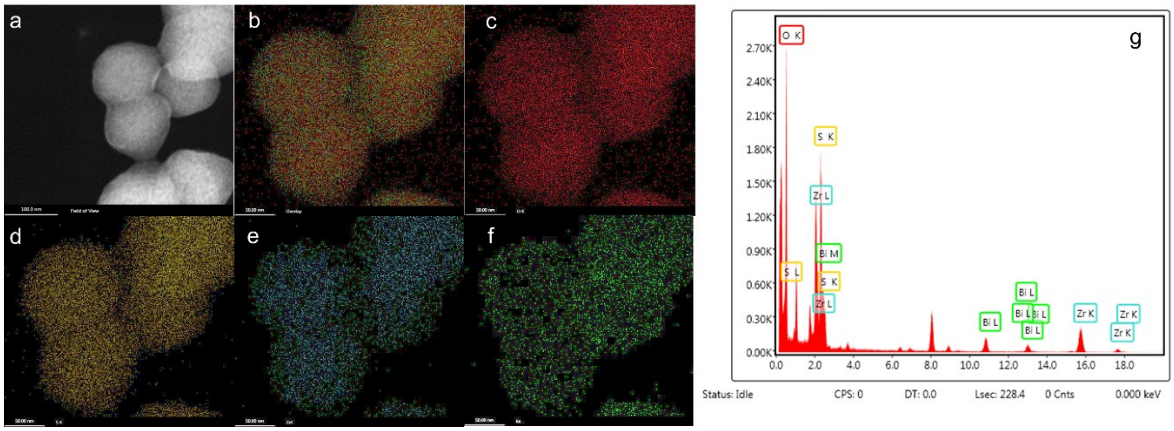

Figure S5. EDX mapping of BiNP@Zr-DMBD-1: a) field of view, b) overlay, c) oxygen, d) sulfur, e) zirconium, f) bismuth, and g) EDX signal spectrum

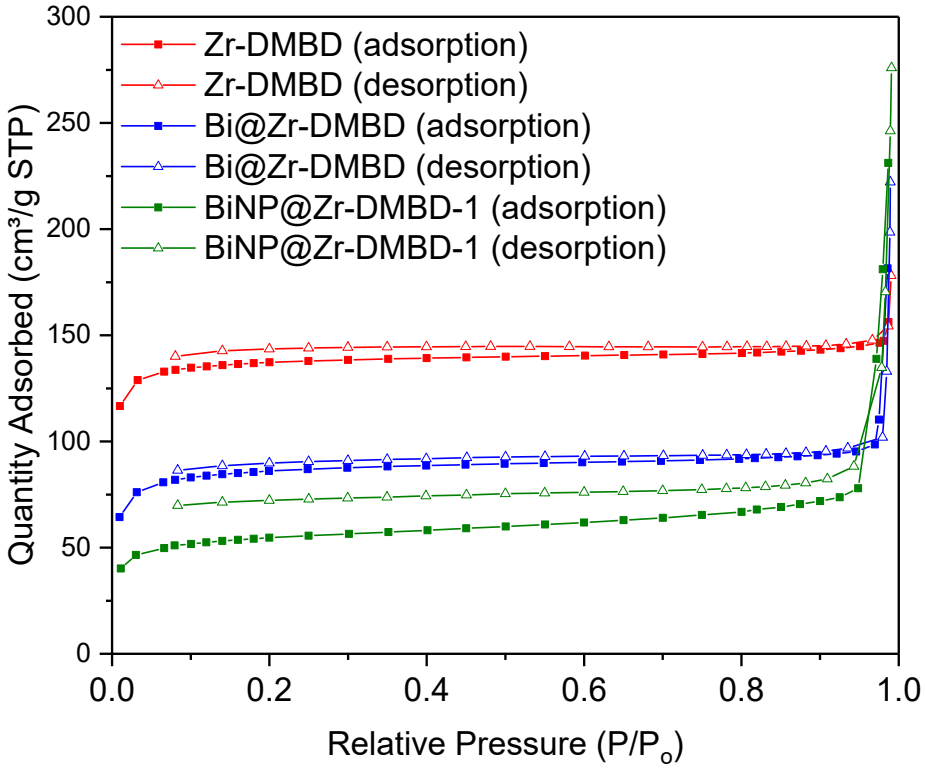

Figure S6. Nitrogen sorption isotherms (77K) of Zr-DMBD (red pattern), Bi@Zr-DMBD (blue pattern), and BiNP@Zr-DMBD-1 (green pattern).

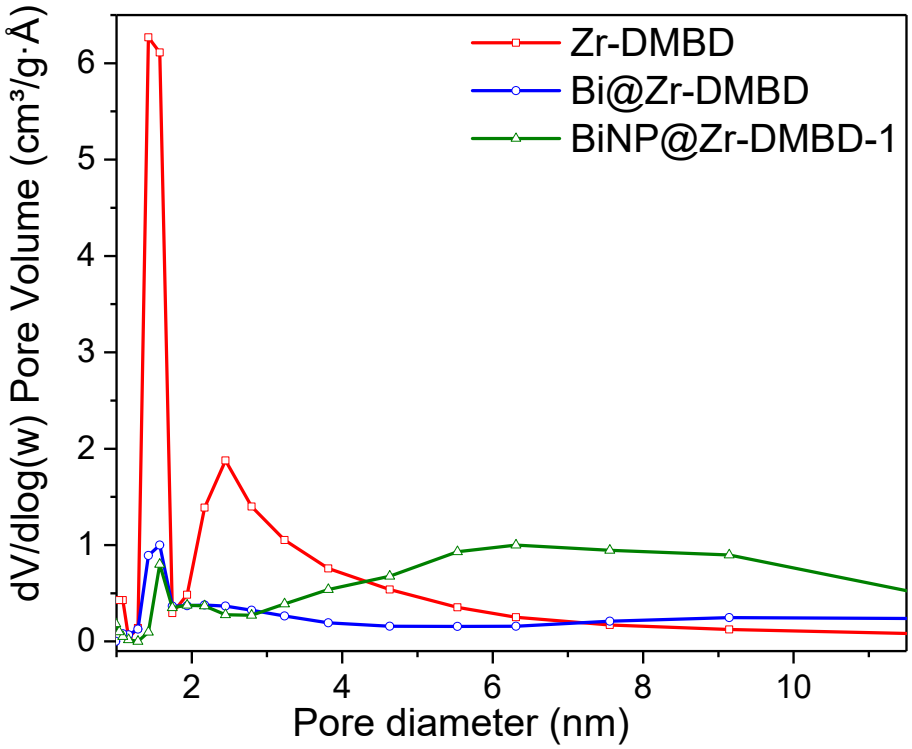

Figure S7. The BJH desorption pore size distribution of Zr-DMBD (red pattern), Bi@Zr-DMBD (blue pattern), and BiNP@Zr-DMBD-1 (green pattern).

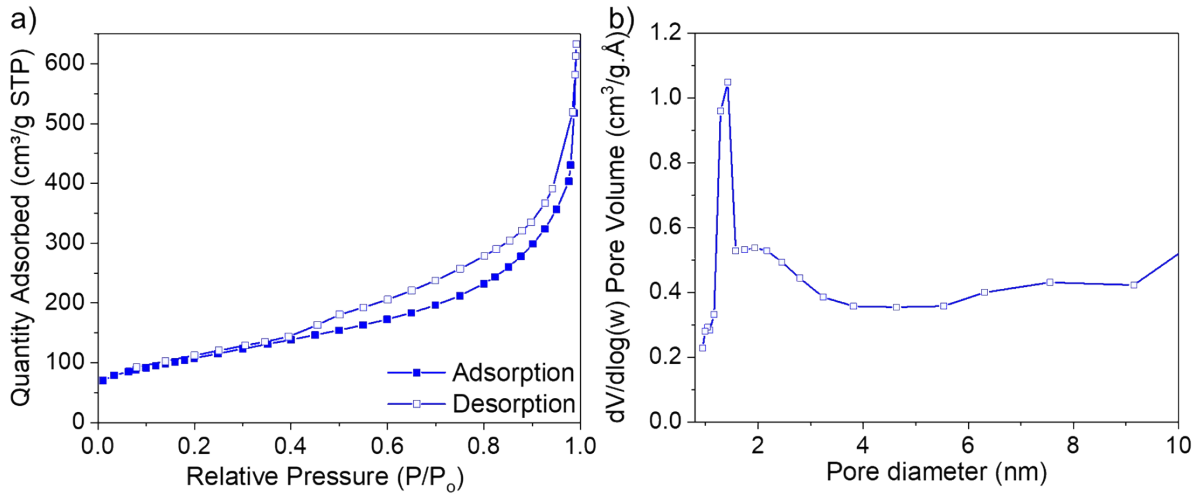

Figure S8. Nitrogen sorption isotherms (77K) and BJH desorption pore size distribution of Zr-DMBD after treatment of $NaBH_4$ (procedure is in the Table S1). The BET surface area was calculated to be 384 $m^2\ g^{-1}$.

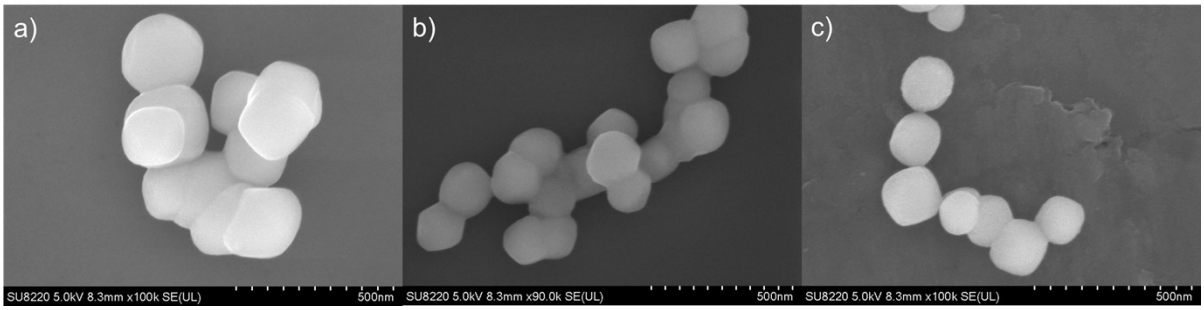

Figure S9. SEM images of (a) Zr-DMBD, (b) Bi@Zr-DMBD, and (c) BiNP@Zr-DMBD-1.

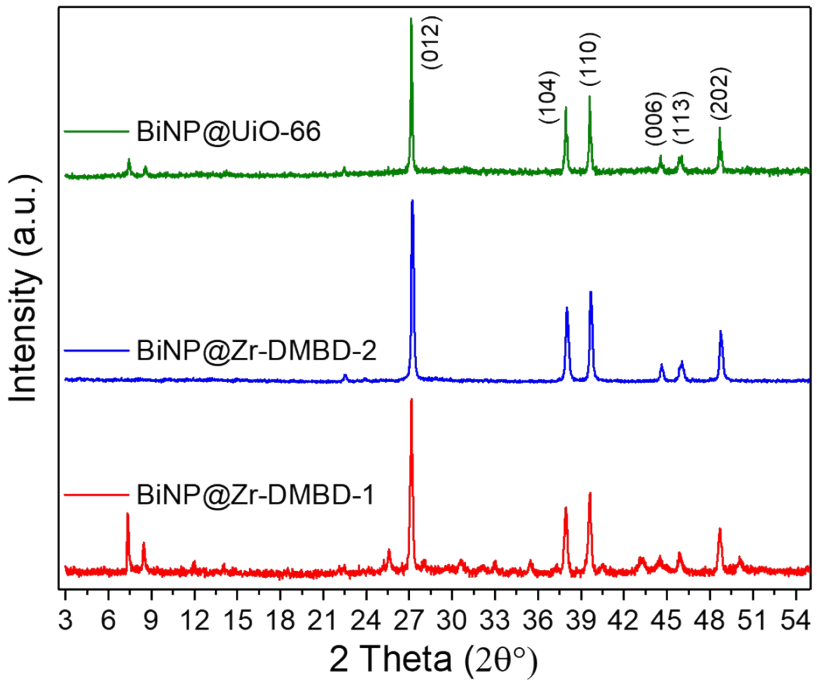

Figure S10. X-ray powder patterns of BiNP@Zr-DMBD-1 (red pattern), BiNP@Zr-DMBD-2 (blue pattern), and BiNP@UiO-66 (green pattern).

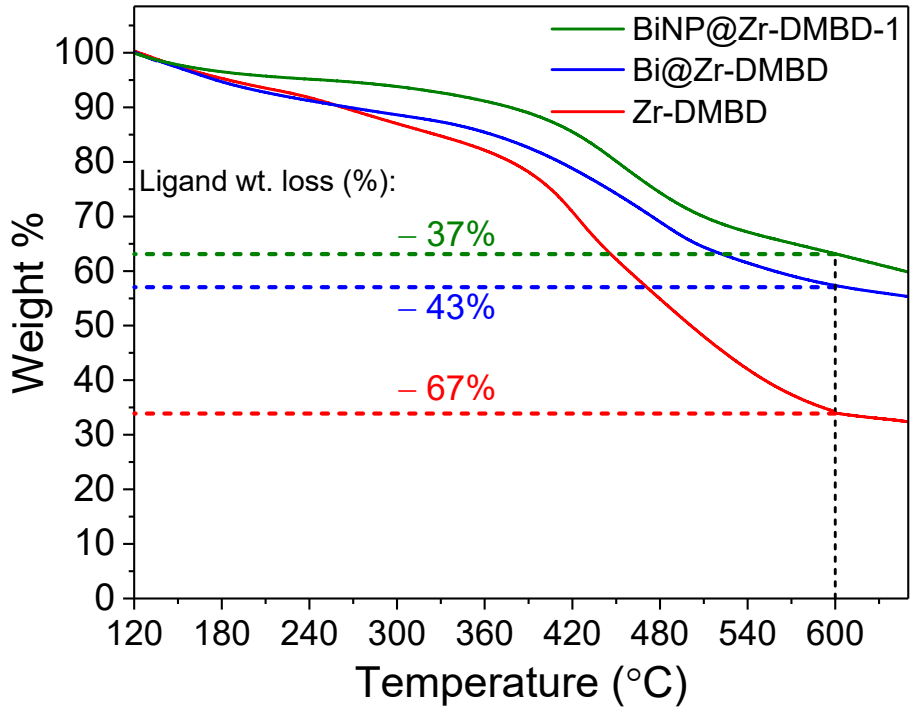

Figure S11. TGA plot of Zr-DMBD (red line), Bi@Zr-DMBD (blue line), and BiNP@Zr-DMBD-1 (green line).

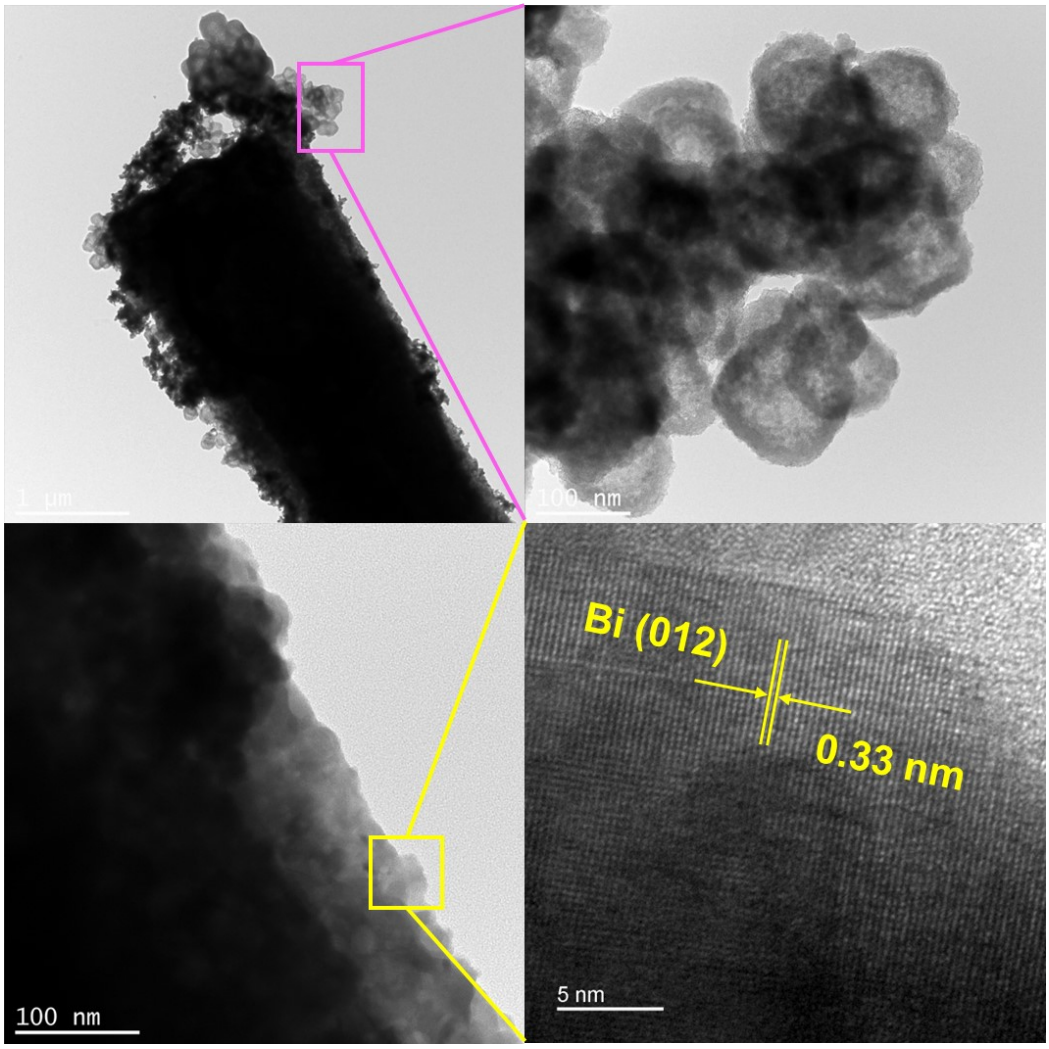

Figure S12. TEM images of BiNP@Zr-DMBD-2 at different scales.

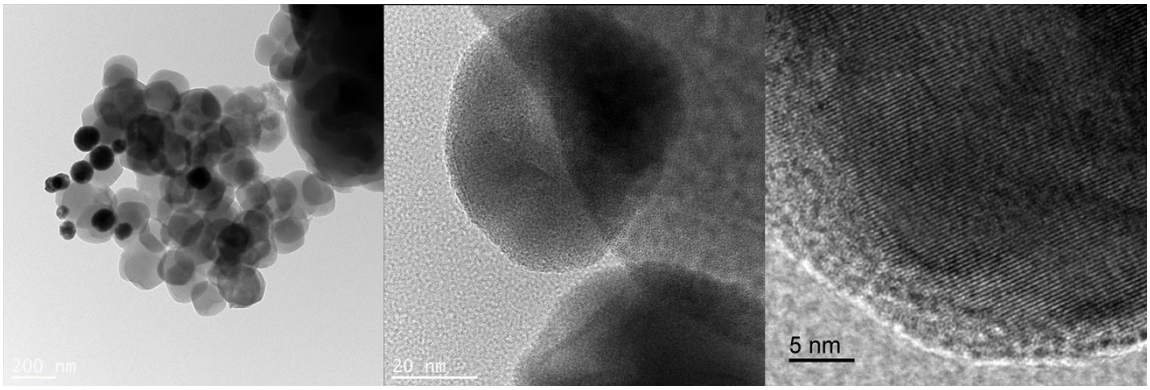

Figure S13. TEM images of BiNP@UiO-66 at different scales.

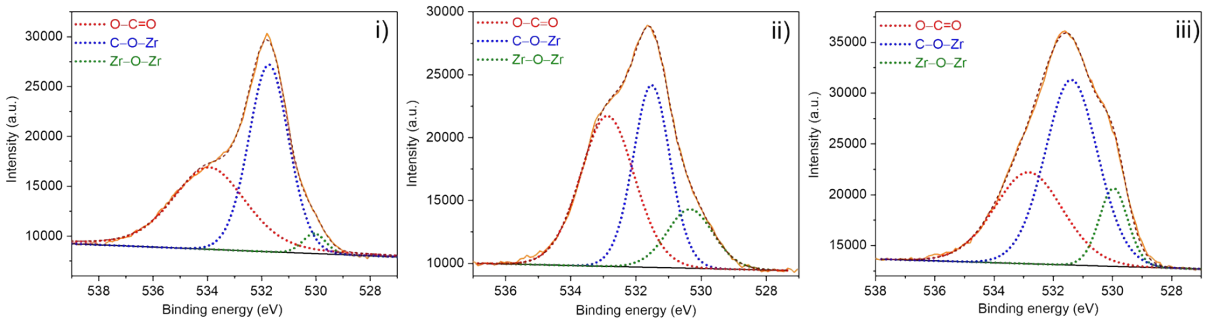

Figure S14. High-resolution O 1s XPS spectra of (i) Zr-DMBD, (ii) Bi@Zr-DMBD, and (iii) BiNP@Zr-DMBD-1, deconvoluted into three constituent peaks of O-C=O, C-O-Zr and Zr-O-Zr.

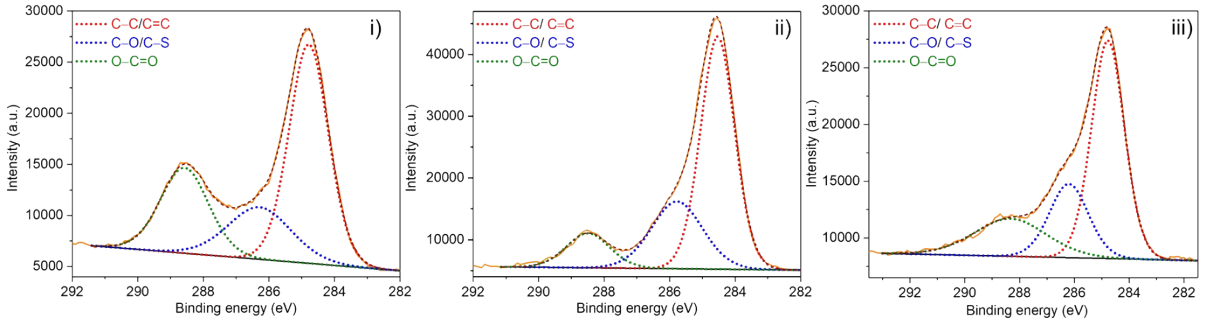

Figure S15. High-resolution C 1s XPS spectra of (i) Zr-DMBD, (ii) Bi@Zr-DMBD, and (iii) BiNP@Zr-DMBD-1, deconvoluted into three constituent peaks of C-C/C=C, C-O/C-S and O-C=O.

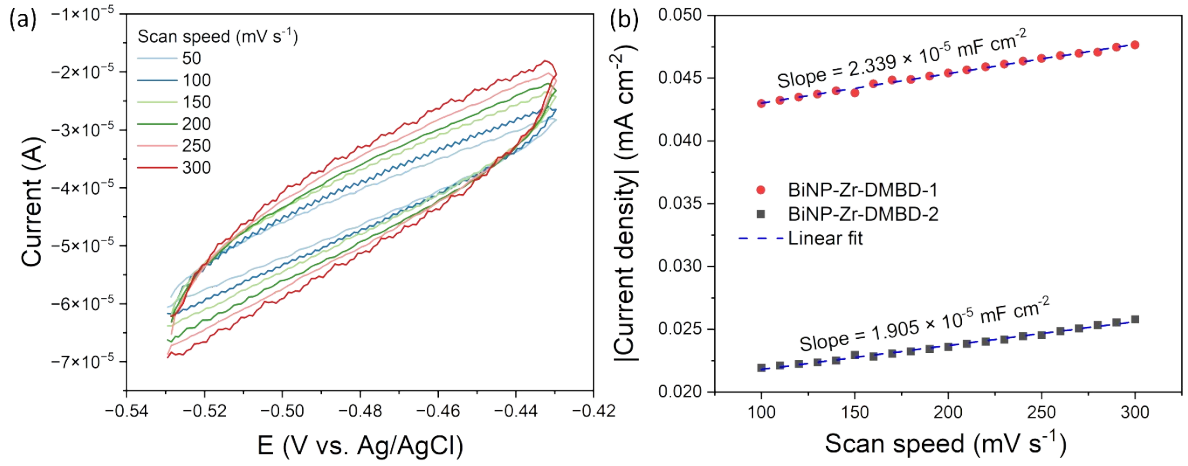

Figure S16. a) Electrochemically active surface area estimation using variable rate cyclic voltammetry measurement. b) Charged double layer (C_{DL}) capacitance (mF/cm^2) of both MOF catalysts, shown as the gradient of the current density vs scan rate graphs. The C_{DL} is used here as an indirect approximation of the ECSA.

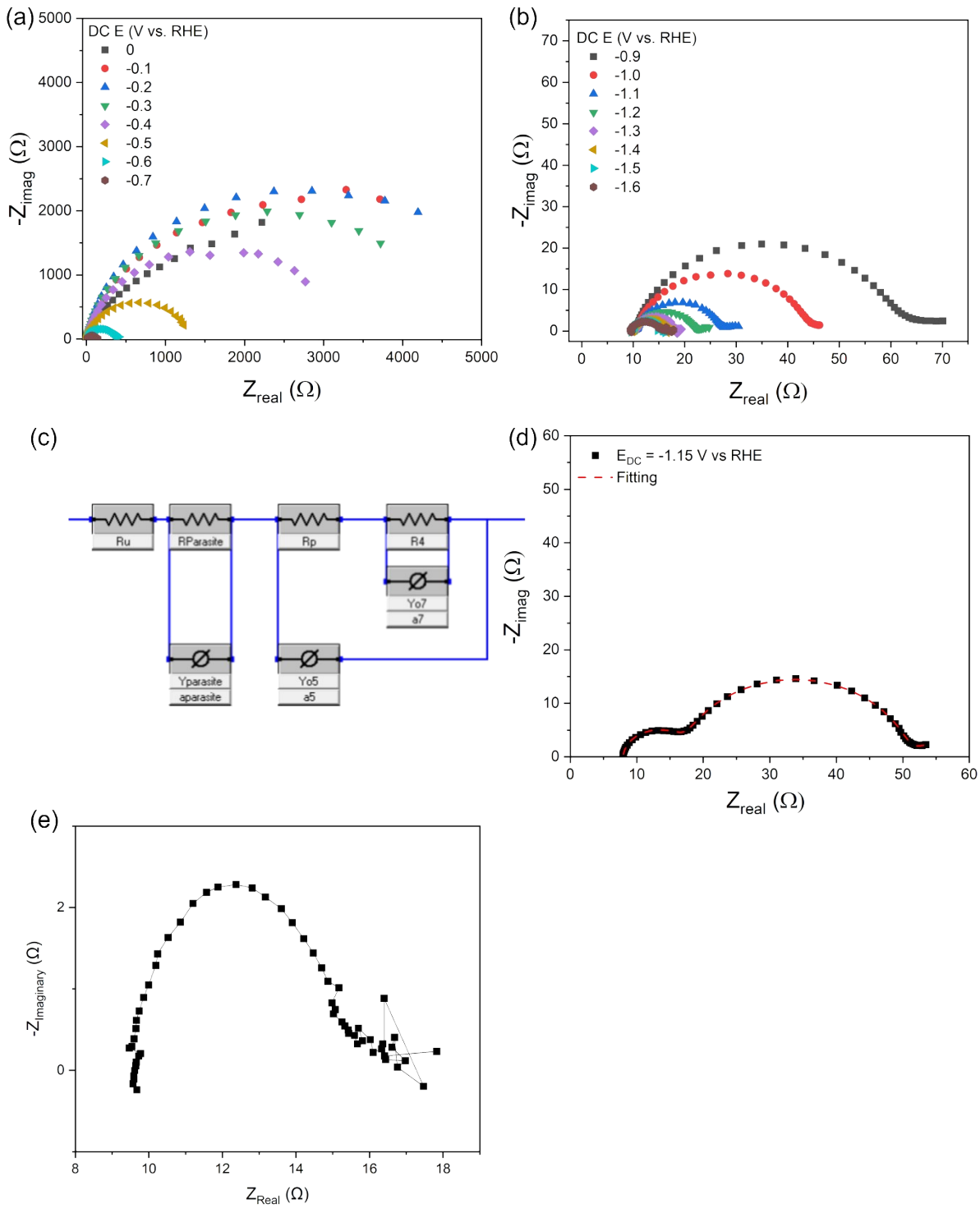

Figure S17. Representative Nyquist plot of BiNP-Zr-DMBD-1 at different DC bias (a) 0 to -0.9 and (b) -0.9 to -1.6 V vs RHE. (c) Modified Armstrong-Henderson equivalent circuit used to fit. (d) Detailed fitting of Nyquist plot at -1.15 V vs. RHE with 3 time constant as shown in Figure C. (e) Magnified section of turbulent EIS datapoints collected at -1.6 V.

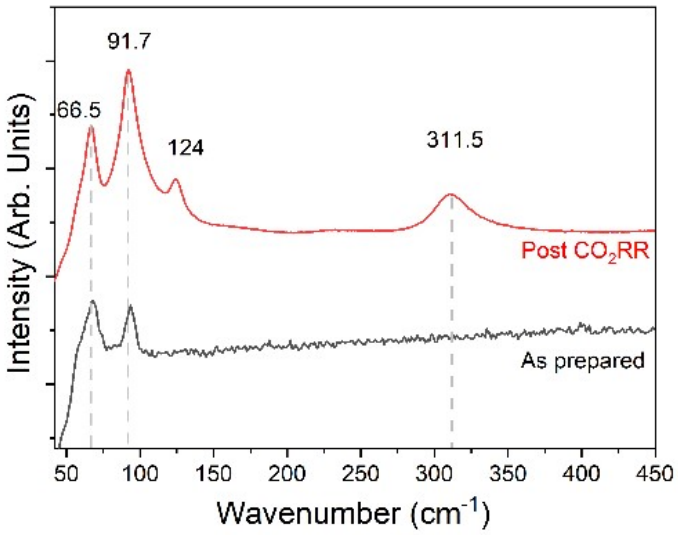

Figure S18. Raman spectra for BiNP@Zr-DMBD-2

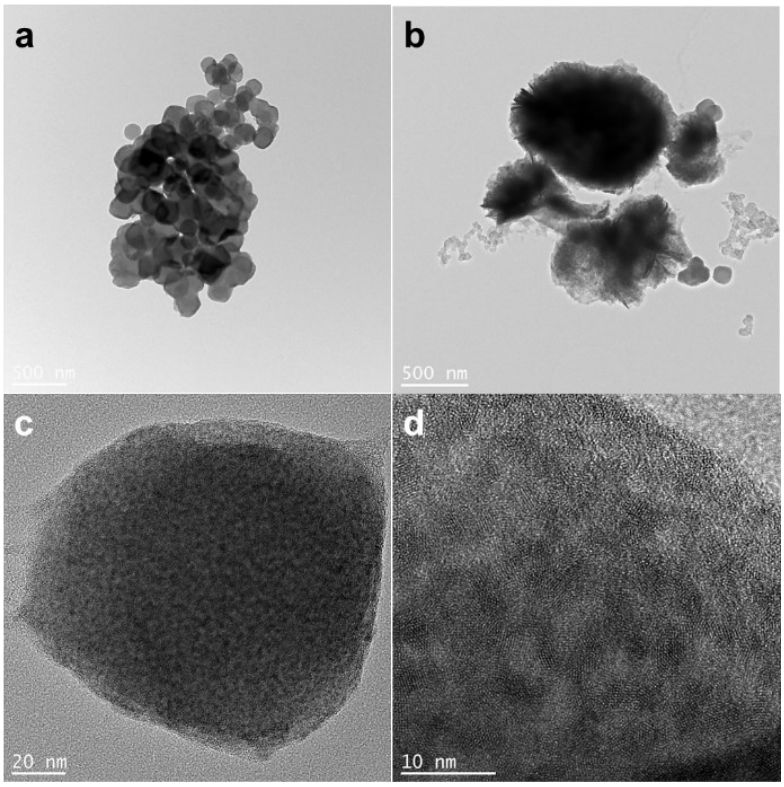

Figure S19. TEM images of recovered BiNP@Zr-DMBD-1 at different scales. (a) and (b) represents uniform sized BiNP@Zr-DMBD-1 and aggregates of Nafion and BiNP@Zr-DMBD-1 respectively. (c) and (d) densely populated BiNPs inside the porous MOF in recovered samples of BiNP@Zr-DMBD-1 post CO_2RR.

XPS based quantification of the constituent elements.

Table S2. XPS based quantification of the constituent elements- Bi, S, and Zr in BiNP@Zr-DMBD-1 before and after CO_2RR.

Element	BiNP@Zr-DMBD-1 Quantification			
	XPS (atom %)		ICP-MS (wt %)	
	As prepared	Post CO_2RR	As prepared	Post CO_2RR wt%
Bi	10.91	14.08	31.5	14.1
S	28.79	-	NA	NA
Zr	60.29	77.16	18.7	7.8
Zr/Bi	12.7	12.6	1.4	1.3

To quantify the constituent elements of BiNP@Zr-DMBD-1 before and after electrochemical CO_2RR, catalytic electrodes were prepared without the presence of any sulphur-containing ionomers like Nafion. Due to an overlap in the S2p and Bi 4f core lines, additional modelling was conducted to discern the contribution of the former to the core line. Figure 7b in the main text demonstrates that the binding energies of the Bi core lines remain in the same region, indicating consistent oxidation states in the catalyst before and after catalysis. Additionally, the modelled XPS core line in Figure S20 reveals the presence of S 2p, which notably decreases post CO_2RR. Quantification of the constituent elements from the XPS data (with adventitious carbon correction applied at 284.8 eV) reveals a significant reduction in sulphur following catalysis, while the ratio of bismuth to zirconium remains consistent post-CO_2RR. No quantitation can be performed reliably for post-CO_2RR sulphur content. This suggests the possibility of selective removal of sulphur-containing organic linkers, particularly from the surface of the BiNP@Zr-DMBD-1 particles, during CO_2RR.

For ICP-MS measurements post CO_2RR, Nafion binder contributes significantly to the collected sample weight, and the results should be taken with caution. Although the absolute wt% for post CO_2RR catalyst is different from as prepared, we believe the ratio of metallic Bi to Zr remains consistent.

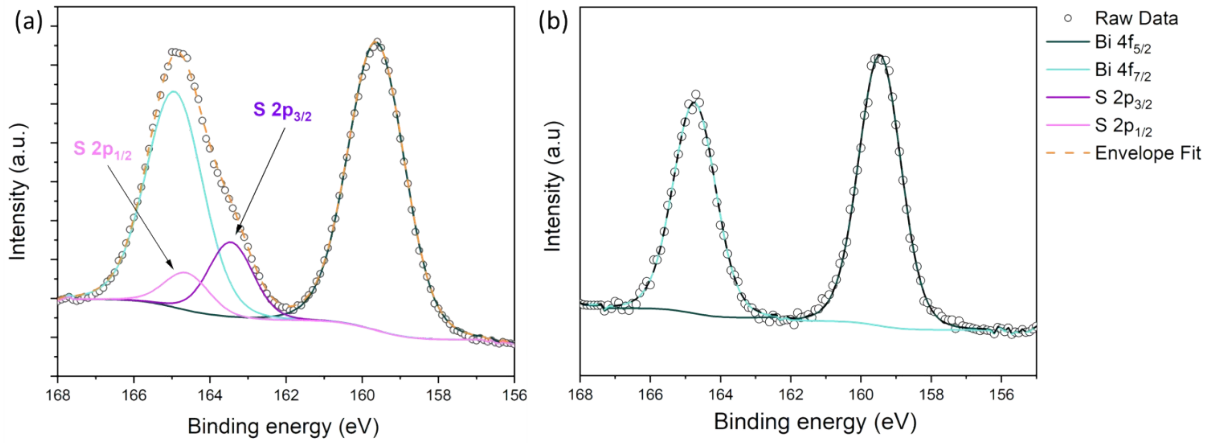

Figure S20. XPS spectra of Bi 4f core line of BiNP@Zr-DMBD-1 without ionomer on glassy carbon (a) as prepared and (b) after CO_2RR. Modelling for the deconvolution of the Bi 4f spectra revealed a reduction in S 2p contribution post-CO_2RR.

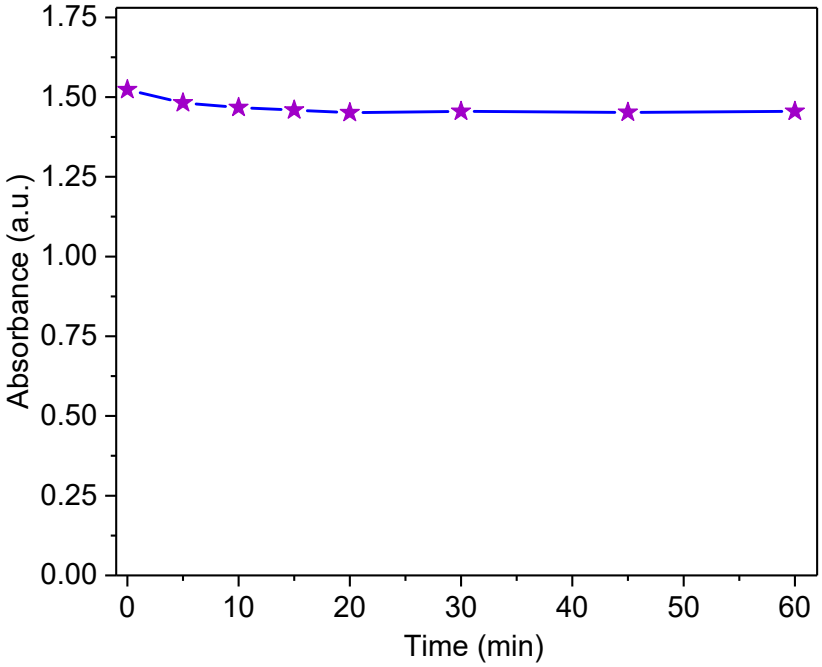

Figure S21. Photodegradation of methylene blue using BiNP@Zr-DMBD-1 in the dark

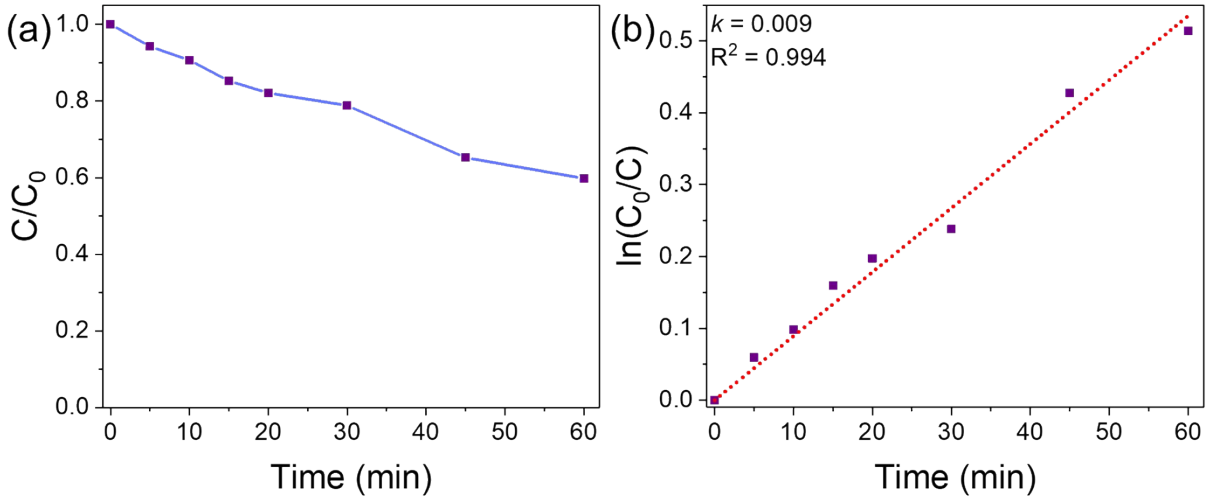

Figure S22. (a) Photodegradation of methylene blue using Zr-DMBD-1 under blue LED light irradiation and (b) the corresponding pseudo first-order rate constants according to the Langmuir-Hinshelwood kinetic model.

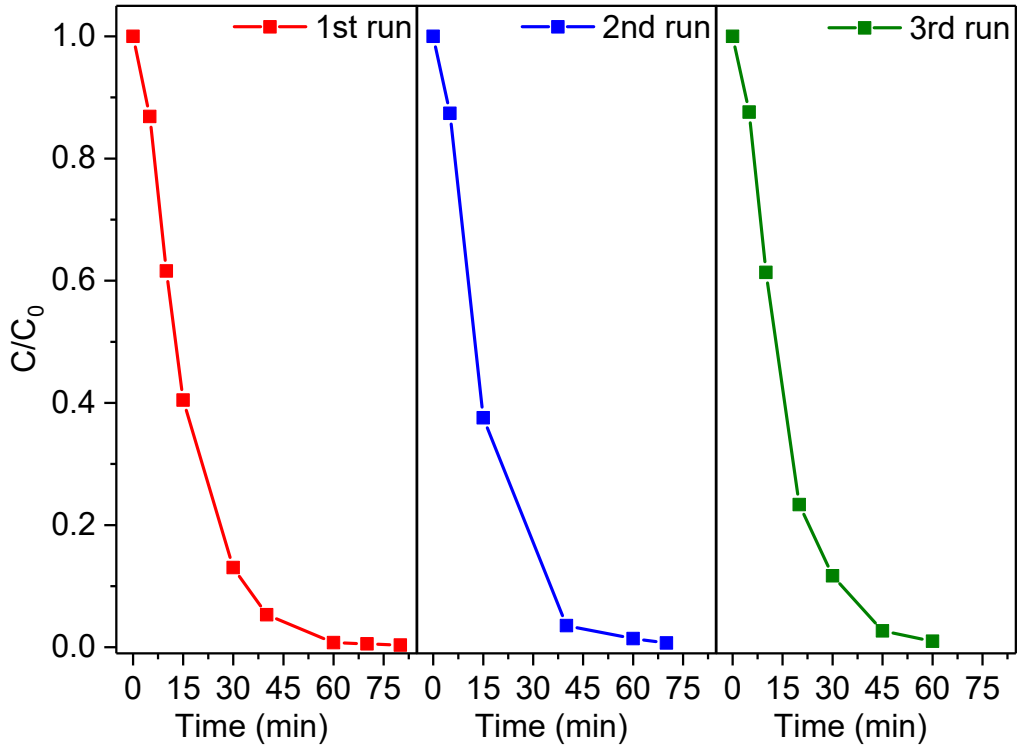

Figure S23. Cycling experiments for the photodegradation of methylene blue using BiNP@Zr-DMBD-1 under standard conditions.

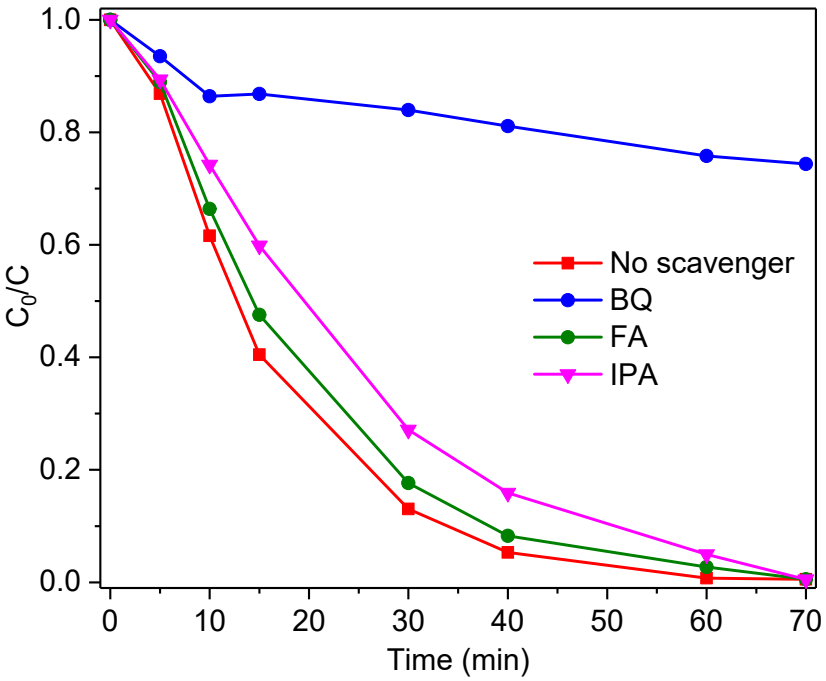

Figure S24. The reactive species quenching study of the photodegradation of methylene blue using BiNP@Zr-DMBD-1 under standard conditions. Scavengers are 1 4 benzoquinone (BQ, blue line), formic acid (FA, olive line), and isopropyl alcohol (IPA, pink line).

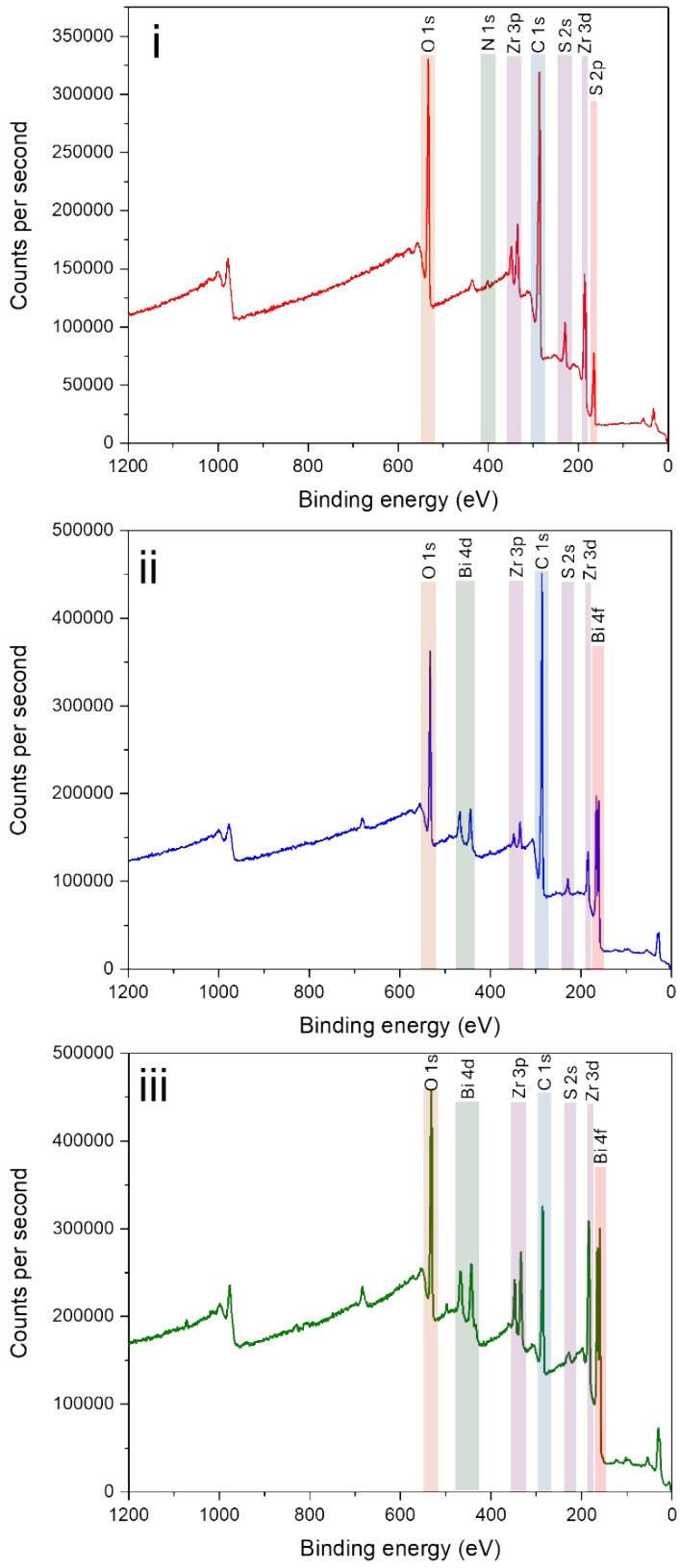

Figure S25. XPS survey of (i) Zr-DMBD, (ii) Bi@Zr-DMBD and (iii) BiNP@Zr-DMBD-1. Little amount of nitrogen in (i) Zr-DMBD is due to the presence of DMF as evident from FT-IR.

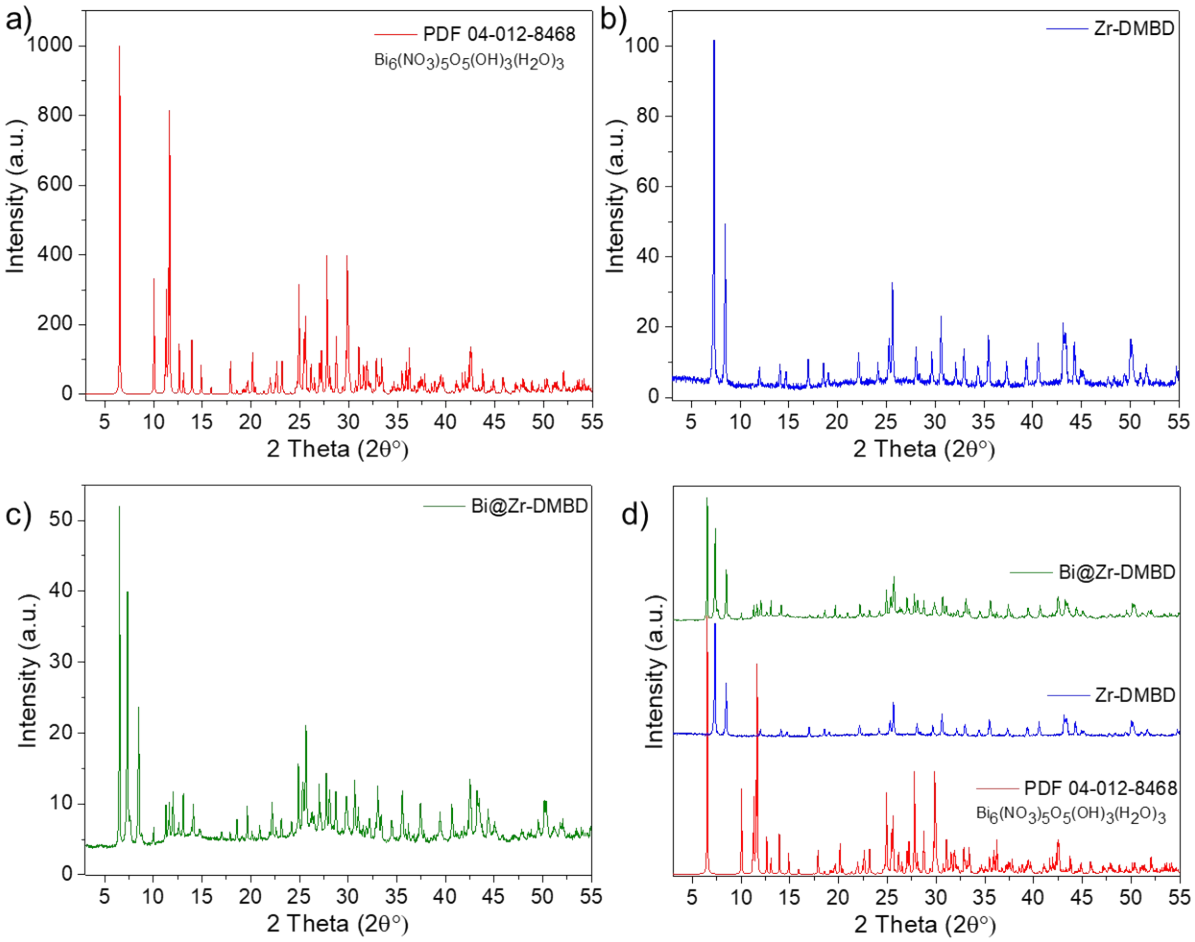

Figure S26. XRD pattern of (a) $Bi_6(NO_3)_5O_5(OH)_3(H_2O)_3$ PDF using DIFFRAC.EVA by Bruker integrated with the DIFFRAC.SUITE database; (b) experimental data of Zr-DMBD; (c) experimental data of Bi@Zr-DMBD; and (d) overlay of XRD patterns.

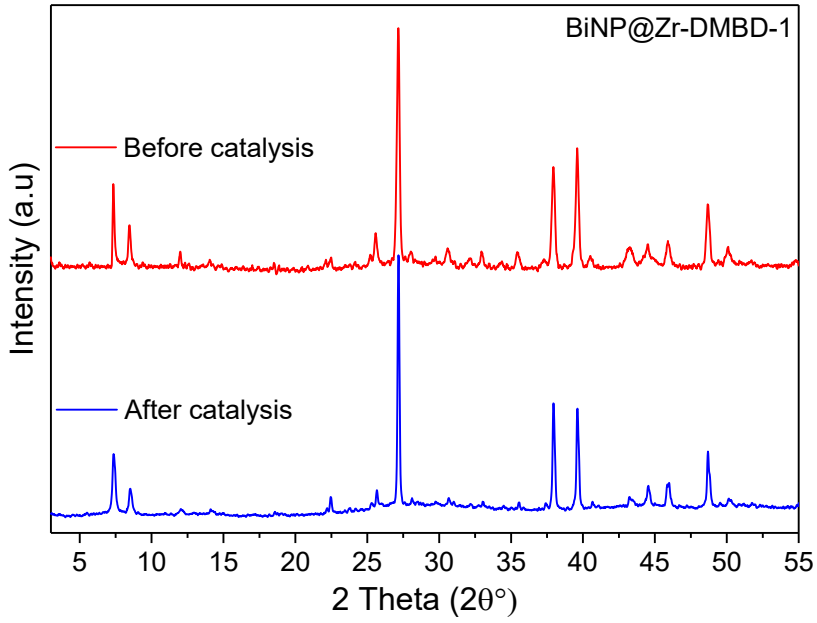

Figure S27. X-ray powder patterns of BiNP@Zr-DMBD-1: as synthesized before photocatalysis (red pattern, top) and recovered after three cycles of photocatalysis (blue pattern, bottom).

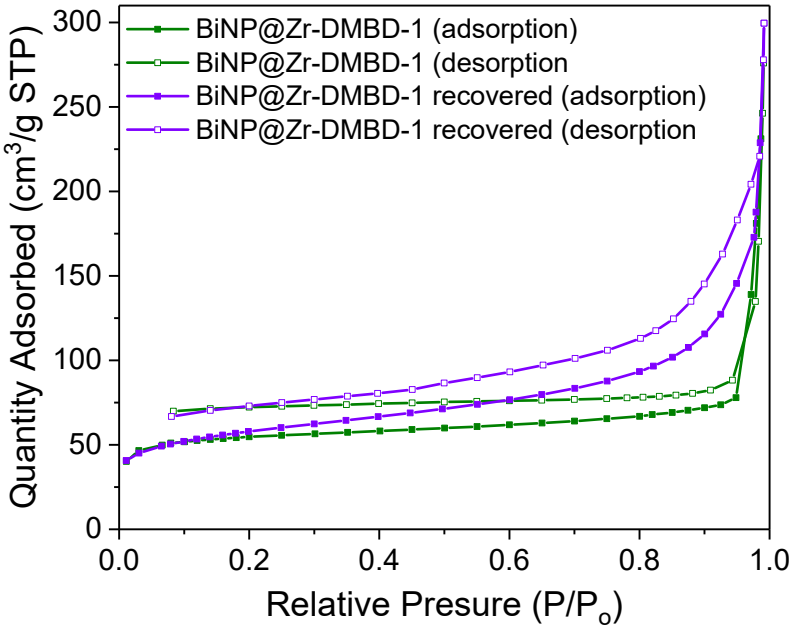

Figure S28. Nitrogen sorption isotherms (77 K) of BiNP@Zr-DMBD-1: as synthesized before photocatalysis (green) with a BET surface area of 199 $m^2 g^{-1}$ and recovered after three cycles of photocatalysis (violet) with a BET surface area of 194 $m^2 g^{-1}$.

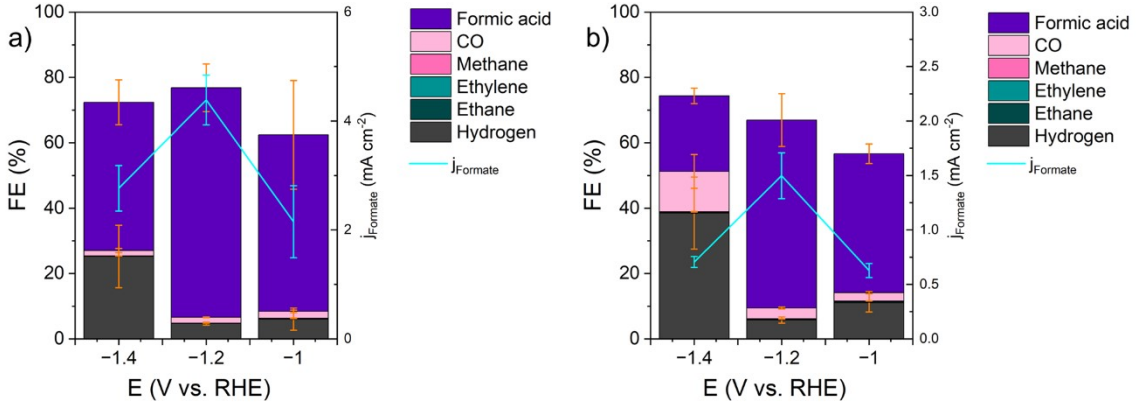

Figure S29: Faradaic efficiencies (FE) of CO_2RR products along with formate partial current density (cyan lines) for (a) Bi@Zr-DMBD and (b) BiNP@UiO-66 electrocatalyst in static H-cell configuration at fixed applied voltage as marked. Vertical orange and cyan bars represent standard deviations of FE and partial current density respectively from 3 independent measurements.